All-porous silicon-coupled microcavities: Experiment versus theory

L. Pavesi
Istituto Nazionale per la Fisica della Materia and Dipartimento di Fisica, Università di Trento, Via Sommarive 14, I-38050 Povo, TN, Italy

G. Panzarini and L. C. Andreani
Istituto Nazionale per la Fisica della Materia and Dipartimento di Fisica ''Alessandro Volta,'' Università di Pavia, Via A. Bassi 6, I-27100 Pavia, Italy

(Received 20 January 1998; revised manuscript received 26 May 1998)

A detailed study of coupled porous silicon (PS) microcavities (PSM's) is reported. The samples are investigated by room temperature photoluminescence and reflectivity. A splitting of the eigenmodes of the coupled cavity structure is observed, as well as a difference between the intensities of the cavity peaks related to mismatch between the two cavity thicknesses. The results are interpreted by a transfer matrix calculation of the optical response of the PSM, where the single PS layer is modeled by Si nanocrystals with a distribution of sizes. Comparison of calculations and experiments allows us to deduce the PS oscillator strength at the band gap. The oscillator strength per cell is found to be $f_{\mathrm{cell}} \sim 4 \times 10^{-5}$, i.e., small, which is consistent with the interpretation of the visible photoluminescence of PS as being due to indirect transitions of quantum confined electrons in Si nanocrystals. [S0163-1829(98)02139-0]

I. INTRODUCTION

The observation of room-temperature photoluminescence in the visible range from porous silicon (PS)[1] has stimulated much research in order to understand the basic mechanism responsible for emission of light, and to develop possible routes towards Si-based optoelectronic devices. The visible PS photoluminescence is believed to be due to electron confinement in low-dimensional Si structures (either undulated quantum wires or quantum dots).[2,3] The nm scale of the Si crystallites gives rise to optical transitions the oscillator strengths of which increase with decreasing nanocrystal size,[4] due to the indirect nature of the bulk Si band gap.

One of the ways to tailor the emission properties of an active medium is to place it in a microcavity with dimensions comparable to an optical wavelength.[5] Semiconductor microcavities are formed by a layer structure similar to a Fabry-Pérot filter: a central active medium is embedded between two dielectric multilayer mirrors. Microcavities allow enhancement or inhibition of spontaneous emission at the energy of the cavity mode to be obtained, together with a highly directional emission; microcavities have been used in VCSEL's (vertical-cavity surface emitting lasers) and diodes with very low threshold.[6,7] Porous silicon microcavities (PSM's) of good quality have been grown, which are superior to PS layers in emission properties.[8–10] In PSM's a double confinement occurs: (1) electron confinement in nanometer-size Si crystallites and (2) photon confinement in optical Fabry-Pérot cavities surrounded by dielectric multilayers [Bragg mirrors, also called distributed Bragg reflectors (DBR's)] made of PS layers with different porosities. The PSM's presented in this work are all made by PS layers.

Recently, coupled cavities made of III-V semiconductors have been grown and characterized.[11–14] These structures consist of two planar Fabry-Pérot microcavities, surrounded by external DBR's and coupled by a central Bragg mirror (see Fig. 1). Coupling of the degenerate cavity modes through the central DBR induced by the long-range, coherent optical field leads to an optical splitting of the eigenmodes.[11,14] Dual lasing has been observed in VCSEL structures containing coupled cavities.[12,13] The coupled cavity structure adds another degree of freedom for the tailoring of spatially confined light-matter coupling; it may lead to interesting effects related to transfer of the excitation from one cavity to another (which is analogous to resonant tunneling in purely electronic systems such as double quantum wells) or to nonlinear control of transmission.

It is interesting to establish to which extent coupled PSM's can parallel the performances of epitaxially grown III-V microcavities. In addition, a study of coupled PSM structures may yield useful information on the mechanism of PS photoluminescence and of the associated oscillator

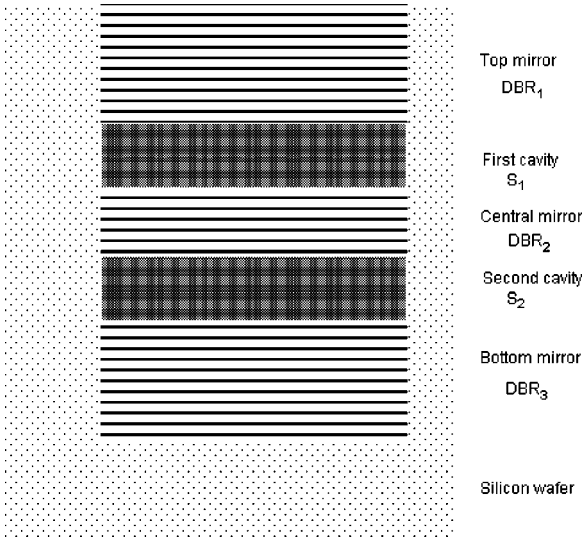

FIG. 1. Schematic sketch of the coupled microcavity structure.

TABLE I. Thicknesses of the two cavity layers (S_1 and S_2) of the various samples, in units of the cavity length λ_c of the balanced sample. λ_1, λ_2, $FWHM_1$, and $FWHM_2$ are the wavelengths and full widths at half-maximum of the first (lower λ) and second (higher λ) cavity resonance, respectively. A_1/A_2 (L_1/L_2) is the ratio between the integrated (peak) emission intensities of the two resonances.

Sample	S_1	S_2	λ_1 (nm)	λ_2 (nm)	$FWHM_1$ (nm)	$FWHM_2$ (nm)	A_1/A_2	L_1/L_2
c	$L_c+L_c/50$	$L_c-L_c/50$	701.4	729.4	5.2	5.5	0.1	0.11
b	$L_c+L_c/100$	$L_c-L_c/100$	734.6	760.5	8.9	8.1	0.42	0.4
a	L_c	L_c	738.9	764.9	4.7	5.7	0.6	0.71
d	$L_c-L_c/100$	$L_c+L_c/100$	733.9	763.0	6.2	6.8	0.96	1.1
e	$L_c-L_c/50$	$L_c+L_c/50$	757.9	784.7	7.4	11.4	0.97	1.5

strength; it also allows a detailed characterization of sample quality and determination of material parameters (index of refraction, the presence of absorption, etc.).

In this work we show that growth of coupled PSM's with good optical properties is possible. We perform photoluminescence and reflectivity experiments for various cavity thicknesses and study the splittings and relative intensities of the spectral structures (associated with the cavity modes and with the sidebands of the Bragg mirrors) and also the trends as a function of a mismatch between the two cavity thicknesses. A theoretical modeling is done by assuming a distribution of oscillators corresponding to emission from Si nanocrystals with different sizes. Particular attention is devoted to the determination of the oscillator strength and other material parameters.

In Sec. II we describe the samples and the experimental procedure. In Sec. III the experimental results are presented. Section IV is devoted to the theoretical model and to the interpretation of the results. Section V contains concluding remarks.

II. EXPERIMENTAL DETAILS

The experimental details on how to construct PSM's are reviewed in detail in Ref. 10. Briefly, PS is formed by an anodic dissolution of a Si wafer in HF. The properties of the resulting PS layer depend on the etching parameters, in particular, the current density determines the porosity of the PS layer and the etching time its layer thickness. As the refractive index, n, of a porous layer is scaled from that of the Si crystal through the porosity, the current density determines the refractive index of the etched PS layer. PSM's are obtained by periodic variations of the current density during the anodic etch of *p*-type doped (0.01 Ω cm) Si wafers. The electrolyte is constituted by an ethanoic solution of HF with an HF concentration of 15% in volume.

Let us call H the high refractive index layer (etching parameters: 1.9 s and 5.75 mA/cm^2) with $n_H=2.24$, L the low refractive index layer (etching parameters: 5.0 s and 49.73 mA/cm^2) with $n_L=1.5$, S_1 and S_2 the first and second cavity (or spacer; etching parameters: 13.03 s and 82.79 mA/cm^2) with $n_c=1.27$. Then the layer sequence used to form the coupled PSM's is as follows: air-$HL \ldots (\times 8) \ldots HL$-$S_1$-$LH \ldots (\times 4.5) \ldots L$-$S_2$-$LH \ldots (\times 8) \ldots LH$ substrate. The final structure is depicted in Fig. 1 and is composed of three DBR's formed by $\lambda/4$ stacks (top mirror DBR_1, central mirror DBR_2, and bottom mirror DBR_3) and two $\lambda/2$ cavity regions, S_1 and S_2. In the balanced PSM, i.e., in a sample where S_1 and S_2 are equal, their thickness is $L_c=\lambda_c/(2n_c)$, where λ_c is the Fabry-Pérot wavelength in vacuum and n_c is the refractive index of the cavity regions (the wavelength of the cavity mode may differ from λ_c due to the dielectric multilayers: see Sec. IV). The various samples are characterized by different values of the thicknesses of S_1 and S_2 as detailed in Table I.

III. OPTICAL SPECTRA OF COUPLED PSMS

In Fig. 2 the reflectivity spectrum of the balanced coupled PSM is shown. The characteristic high reflectivity region due to the stop band of the three DBR's extends from about 620 to 840 nm, as indicated by the two pronounced reflectivity minima. Note, however, that two weaker structures around 650 and 800 nm are present: they should not be taken as indications of a narrower stop band, and are rather due to structural disorder in the DBR's, as discussed for similar structures in Ref. 10 and in the next section. Within the wavelength (λ) region of the stop band, two reflectivity resonances are observed at 739 and 765 nm due to the resonant coupling between the optical modes confined in the first and second cavity. A maximum transmittivity of 0.44 and 0.27 is associated with the low and high λ resonance, respectively. Even though the two cavities are equal, a different transmittivity is observed due to the residual absorption of the central DBR at these wavelengths.

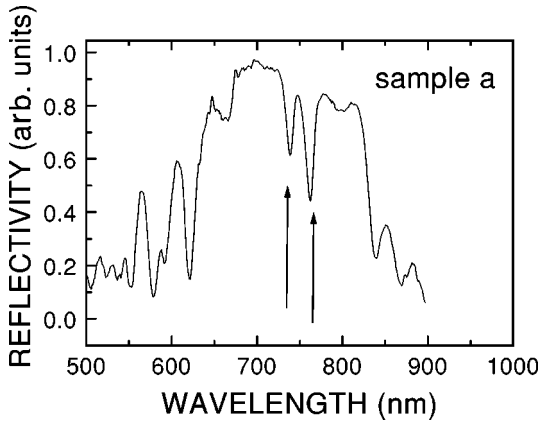

FIG. 2. Reflectance spectrum of the balanced all-porous silicon-coupled microcavity (sample *a*). The arrows point to the cavity modes.

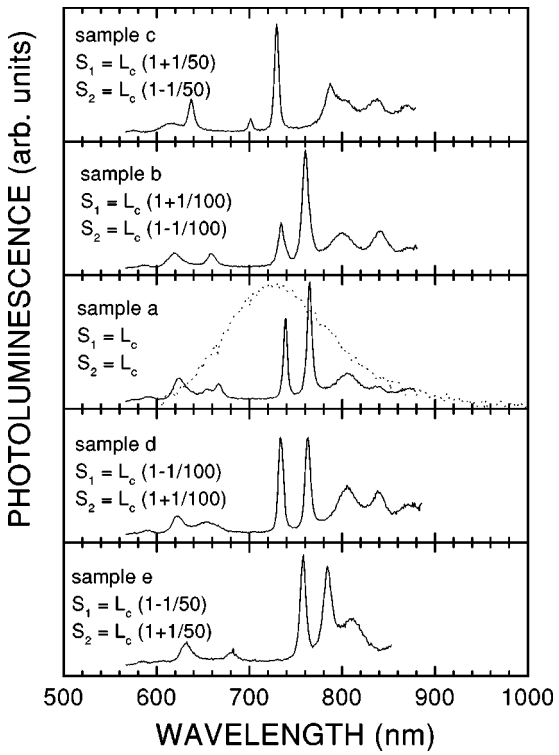

FIG. 3. Luminescence spectra of coupled microcavities for the various thicknesses of the cavity layers (S_1 and S_2) indicated on the left. The spectra are in relative units. The dotted line in the central panel refers to a luminescence spectrum of a reference PS sample grown with the same etching parameters as the cavity layers. The spectrum has been normalized to its maximum and should be multiplied by a factor 0.09 to be reduced to the same relative units of the spectrum of the PSM.

In order to study the coupled PSM in a deeper way, a series of samples with different mismatch between the two cavity layers has been studied. Figure 3 shows the photoluminescence spectra at room temperature for the various samples. Some information extracted from these spectra is also summarized in Table I.

The overall shape of the luminescence spectra is similar for all samples and very different from the typical one of PS. As a comparison in Fig. 3 central panel, the luminescence of a PS sample etched with the same parameters of the cavity layers is reported. Instead of the characteristic wide emission band of PS, in PSM's several peaks are observed corresponding to the reflectivity minima of the PSM structure (see, e.g., Fig. 2). At the wavelengths of the coupled cavity modes, two narrow and sharp peaks are observed, the intensities of which depend on the mismatch between the S_1 and S_2 cavities. The emission in the stop band is not completely flat, since several peaks are present: note, in particular, that the structures at 650 and 800 nm of sample *a*, which correspond to the weak reflectivity structures in Fig. 2, are much more prominent in PL than in reflectivity. Therefore the size of the stop band cannot be derived from PL. The peculiar features of the PSM luminescence compared to that of PS are a consequence of the photon confinement in the cavity structure and have been discussed at length in Refs. 8–10.

Here we concentrate on the phenomena introduced by the coupled cavity structure. For the balanced sample labeled *a* (central spectrum in Fig. 3), two narrow peaks are observed at 739 and 765 nm corresponding to the transmittivity maxima measured in the reflectivity spectrum shown in Fig. 2. They are therefore the fingerprint of the two coupled cavity modes, which have an equal probability of being localized in each of the two cavities. By varying the mismatch between S_1 and S_2, several features can be observed:

(1) The growth process is well controlled as similar spectra are observed for the various samples, so we can conclude that the variations are due to the different etching parameters used.

(2) The peak intensities vary as a function of ΔL_c (the thickness difference between S_1 and S_2). In particular, the high λ peak is strongest for sample *c* and the low λ peak is strongest for sample *e*. In the balanced sample *a*, an intensity difference between the emission of the two cavity modes (hereafter referred to as ''intensity asymmetry'') is observed due to a residual absorption present in the structure and to the wavelength dependence of the PS emission band.

(3) The spectral position does not change as a function of ΔL_c, except for sample *c* (sample *e*), where the two cavity peaks as well as the sidebands are shifted to shorter (longer) wavelengths.

(4) The linewidth of the luminescence peaks is almost independent of ΔL_c and significantly smaller than that typical of PS.[9]

IV. THEORETICAL MODELING OF COUPLED PSMS

The theoretical modeling of the experimental results is done by assuming a dielectric function $\epsilon(\omega)=\epsilon_\infty+4\pi\chi(\omega)$ in each layer, where $\epsilon_\infty=n^2$ is the background dielectric constant, and $\chi(\omega)$ is a resonant contribution arising from optical transitions close to the band gap. We assume for each PS layer a model of nanocrystals with a dispersion of sizes, and take the energies of spatially confined oscillators to be distributed according to a Gaussian function centered at ω_0:

$$P(\omega)=\frac{1}{\Delta\sqrt{\pi}}\exp\left(-\frac{(\omega-\omega_0)^2}{\Delta^2}\right). \tag{1}$$

The width Δ of the distribution corresponds to the width of the bulk PS photoluminescence.[10] Both ω_0 and Δ depend on the porosity, with a trend of increasing ω_0 for increasing porosity, probably due to a smaller size for the Si nanocrystals. However, since the distribution of the PS photoluminescence is much larger than the energy range of interest (i.e., it extends well outside the stop band of the PSM structure), for the sake of simplicity we assume the same values for all PS layers. In fact, the results shown below do not depend on the precise form of the resonance frequency distribution: a different form as assumed in Ref. 8 yields very similar results. The resonant susceptibility is then obtained by a convolution of the single-oscillator form with the resonance frequency distribution:

$$\chi(\omega)=\int_{-\infty}^{\infty}P(x)\frac{\beta x^2}{x^2-\omega^2-2i\gamma\omega}dx. \tag{2}$$

The susceptibility (2) can be expressed in terms of the complementary error function. Reflectivity and absorption spectra are then calculated by solving Maxwell equations with the usual transfer-matrix method.[16,17] The parameters of the oscillator model are taken as $\hbar\omega_0 = 1.65$ eV ($\lambda_0 = 750$ nm), $\Delta = 285$ meV, $\gamma = 15$ meV.

Although the nominal refractive indices and layer thicknesses are determined by the growth parameters, their values for a single layer may be modified in the presence of a multilayer structure, as discussed in Ref. 10. Thus we allow for small deviations from the nominal growth parameters in order to give a better description of the experimental results. Figure 2 shows that the wavelength of the isolated cavity modes, taken as the average of the two peaks, is $\lambda_m = 753$ nm; the center of the stop band is instead at $\lambda_s = 713$ nm.[15] Thus the cavity mode is at longer wavelengths than the center of the stop band. In general, the frequency ω_m of the cavity mode is a weighted average of the bare Fabry-Pérot frequency $\omega_c = 2\pi c/n_c L_c$ and the center of the stop band ω_s:

$$\omega_m = \frac{L_c\omega_c + L_{\mathrm{DBR}}\omega_s}{L_c + L_{\mathrm{DBR}}}, \tag{3}$$

where L_{DBR} is a penetration depth in the dielectric mirrors. Thus we conclude that the cavity length L_c, which determines the bare Fabry-Pérot frequency, must be higher than $\lambda/2$. Keeping the refractive indices at the nominal growth values, but allowing for different values of the layer thicknesses, we get the following set of parameters: $L_c = 347$ nm for the length of the balanced cavity and $n_c = 1.27$ for the cavity refractive index; $a = 118.9$ nm, $b = 79.6$ nm for the DBR layer thicknesses, and $n_L = 1.5$, $n_H = 2.24$ for the respective refractive indices. The external (central) DBR have $N_1 = N_3 = 8$ ($N_2 = 4.5$) pairs, respectively.

Useful analytic results for the double-microcavity configuration can be obtained by parametrizing the transfer matrix of the Bragg mirrors in terms of their amplitude reflection coefficients: this allows to obtain the transfer matrix of the whole structure, and to calculate the energies of the system eigenmodes as the poles of the global transmission coefficient $t(\omega)$ (the procedure was first applied to single microcavities in Ref. 18). For a structure with two identical cavities, the optically coupled Fabry-Pérot modes can be classified in terms of their symmetric (S) and antisymmetric (A) states; their splitting at normal incidence is calculated as

$$\Delta_{\mathrm{S-A}} = \frac{\hbar c\sqrt{1-R_2}}{n_c L_{\mathrm{eff}}}, \tag{4}$$

where $R_2 = 1 - 4(n_H/n_c)^2(n_L/n_H)^{2N_2+1}$ is the reflectivity of the central mirror, and $L_{\mathrm{eff}} = L_c + L_{\mathrm{DBR}}$ is an effective cavity length. Using the approximate formula $L_{\mathrm{DBR}} = 2(n_L n_H/n_c)^2(a+b)/(n_H^2 - n_L^2)$,[17,14] we find $L_{\mathrm{eff}} = 1.35\,\mu$m and $\Delta_{\mathrm{S-A}} = 54.5$ meV: this agrees well with the experimental splitting of about 55 meV shown in Fig. 2. This comparison shows that coherence of the optical field is maintained over the whole thickness of the central DBR, and therefore that the PSM's have a good quality that enables us to observe coherent coupling effects of the kind first reported for III-V coupled microcavities.[11]

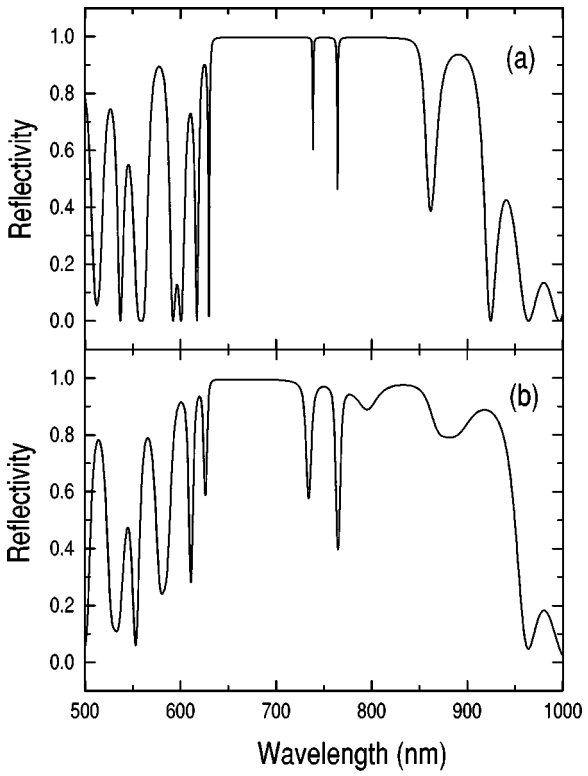

FIG. 4. Calculated reflectivity spectra for the balanced sample *a*. (a) ''Ideal'' sample. (b) Including the effect of PS oxidation, the background absorption, and the spread of the refractive indices (see text).

In Fig. 4(a) we show the calculated reflectivity for the balanced sample *a*, with the above set of parameters (and with $\beta = 3\times10^{-5}$: see below). Comparing with Fig. 2, we see that the positions of the cavity dips and the width of the stop band are correctly reproduced. The relative intensities of the two dips, which are similar to the experimentally observed ones, arise from the presence of absorption in the PS layer: a more detailed discussion is given below. As a general remark, we also notice that the reflectivity spectra have a weak dependence on the parameters of the PS oscillators: the coupled cavity dips are determined by the phase-matching condition in each cavity and by the optical coupling, and therefore depend mainly on the real part of the refractive indices. In particular, the position of the cavity dips is almost independent of the oscillator strength: even for $\beta = 0$ (i.e., no oscillators in the PS layers) coupled cavity dips would occur at the same positions.

Comparing the cavity dips in Fig. 4(a) with the experimental ones in Fig. 2, a discrepancy concerning the linewidth can be noticed: the theoretical dips are too narrow. The peak line shape depends on the precise values of the refractive indices, in particular the linewidth depends on the reflectivity of the external DBR's and is sensitive to the contrast between n_H and n_L. Since PS undergoes a very fast and uncontrolled aging process, we have tried to include this effect in the calculations by reducing the contrast of the refractive indices of the layers of the outermost DBR. This will mimic a progressive oxidation of the structure. In addition, we have included nonresonant absorption in all PS layers by adding a small imaginary part to the refractive indices, and have assumed the real parts of the refractive indices to be inhomo-

geneously distributed according to a Gaussian law: by this procedure, which accounts for lateral inhomogeneities in the sample, it was found that even a very small($\sim 10^{-3}$) spread of the refractive indices yields a large broadening of the spectra. The result of this simulation for the reflectivity is shown in Fig. 4(b). It can be seen that the cavity dips are much wider, in better agreement with the experimental data shown in Fig. 2, while the dip positions and the width of the stop band are unchanged; in addition, the new material parameters yield weak reflectivity features in the stop band, which resemble the experimental ones. We stress once more that the dip area is unrelated to the oscillator strength of the PS emitters. Since the precise peak line shape depends on a number of unknown material parameters, while it does not yield any crucial physical information, in the following we stick to the ''ideal'' structural parameters of Fig. 4(a) and do not attempt to reproduce the experimental linewidth.

The parameter β appearing in Eq. (2) is proportional to the oscillator strength of the optical transitions in the nanocrystals; a determination of β is now made by comparing the experimental PL with the calculated absorption spectrum. Although the two spectra are related by the principle of detailed balance, one might wonder about possible thermal effects in the PL spectrum. In the present framework each PS layer is viewed as a set of weakly interconnected quantum dots with a size distribution; since the PL line of bulk PS is inhomogeneously broadened, there is no reason why thermalization between independent dots should occur. Indeed, the nearly symmetric line shapes of the PS luminescence spectra indicate that there is no thermalization in the occupation of high-energy states, unlike in other semiconductor systems. Moreover, for our multilayer structure all cavity and DBR layers are assumed to have the same size distribution and are treated on equal footing: thus a calculation of absorption is expected to give a fair description of PL spectra, with the relative oscillator strengths of the various regions of the spectrum being well accounted for.

When comparing with PL measurements, where only the lowest-lying states of each nanocrystal are probed, β has to be interpreted (to within a multiplicative factor) as the oscillator strength *at the band gap* for each nanocrystal in the corresponding PS layer, averaged over the inhomogeneous size distribution. This oscillator strength is known to decrease with nanocrystal size,[4] since it must go to zero in the limit of a bulk Si crystal with indirect gap. A quantitative determination of the oscillator strength is one of the main purposes of this work. In Fig. 5, the calculated absorption for different values of the parameter β (which for simplicity is taken to be frequency independent and the same in all layers) is shown. When $\beta<10^{-5}$ absorption is concentrated in the cavity peaks, while for $\beta>10^{-4}$ most of the absorption takes place in the side bands of the mirrors. Note that the cavity absorption is not a monotonically increasing function of β: when β gets larger than $\sim 10^{-5}$ and increases towards unity, the quality factor of the cavity is degraded and absorption at the cavity peaks decreases. The experimental indication that the PL intensities of all peaks are comparable (see Fig. 3) points to an optimal value of β between 10^{-5} and 10^{-4}. In the following, a value $\beta=3\times10^{-5}$ is assumed.

The parameter β is related to the oscillator strength by

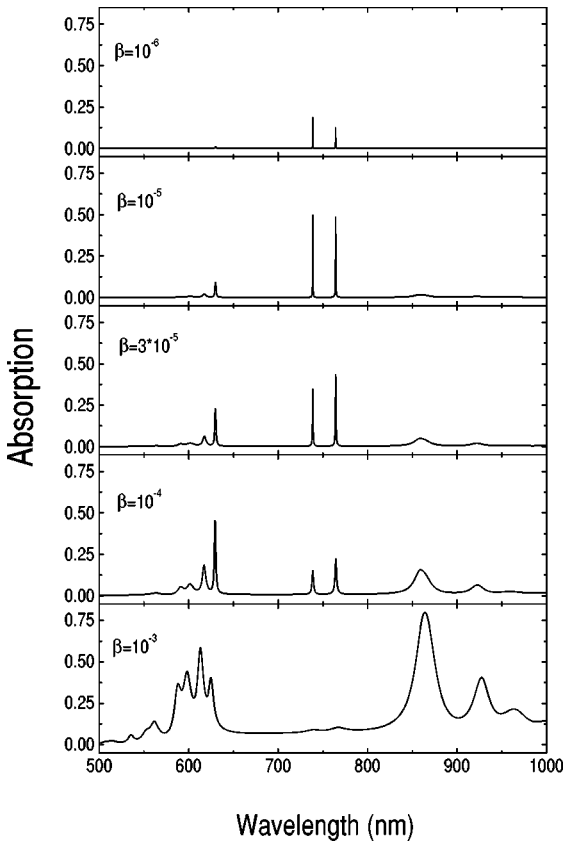

FIG. 5. Absorption of a balanced coupled microcavity as a function of the parameter β [Eq. (4)]. The structure is the same as that used experimentally in Fig. 2; parameters of the calculation are given in the text.

$$\beta=\frac{e^2}{m\omega_0^2}\frac{f}{V}, \tag{5}$$

where f/V is the oscillator strength per unit volume. Taking the volume of a unit cell, the oscillator strength per cell $f_{\text{cell}}\simeq 4\times10^{-5}$. This compares well with the values calculated by Delley and Steigmeier[4] for the larger nanocrystals. Also, with this value for the oscillator strength a radiative decay rate $\Gamma=2ne^2\omega^2 f_{\text{cell}}/(3mc^3)\sim 2\ \text{ms}^{-1}$ is obtained, close to the values calculated in Ref. 3 for a gap of 1.6 eV. Thus we may conclude that the present PSM structures are characterized by nanocrystals with a small oscillator strength; this is consistent with the explanation of the visible PL band in terms of radiative recombination of electron-hole pairs (or excitons) at the band gap of Si nanocrystals, with a slow radiative lifetime in the ms range.

In Fig. 6, the calculated absorption (a) and reflectivity (b) for the parameters of the five samples are reported. The intensity asymmetry of the two cavity peaks for the balanced sample *a*, which reproduces the observed one, is due to the presence of absorption. It is important to notice that if the refractive index is real, a cavity mismatch alone does not yield a different intensity of luminescence peaks or of reflectivity dips; on the other hand, a complex refractive index does produce an intensity asymmetry, which depends strongly on the mismatch between the two cavities. In our case the imaginary part of the refractive index is provided by

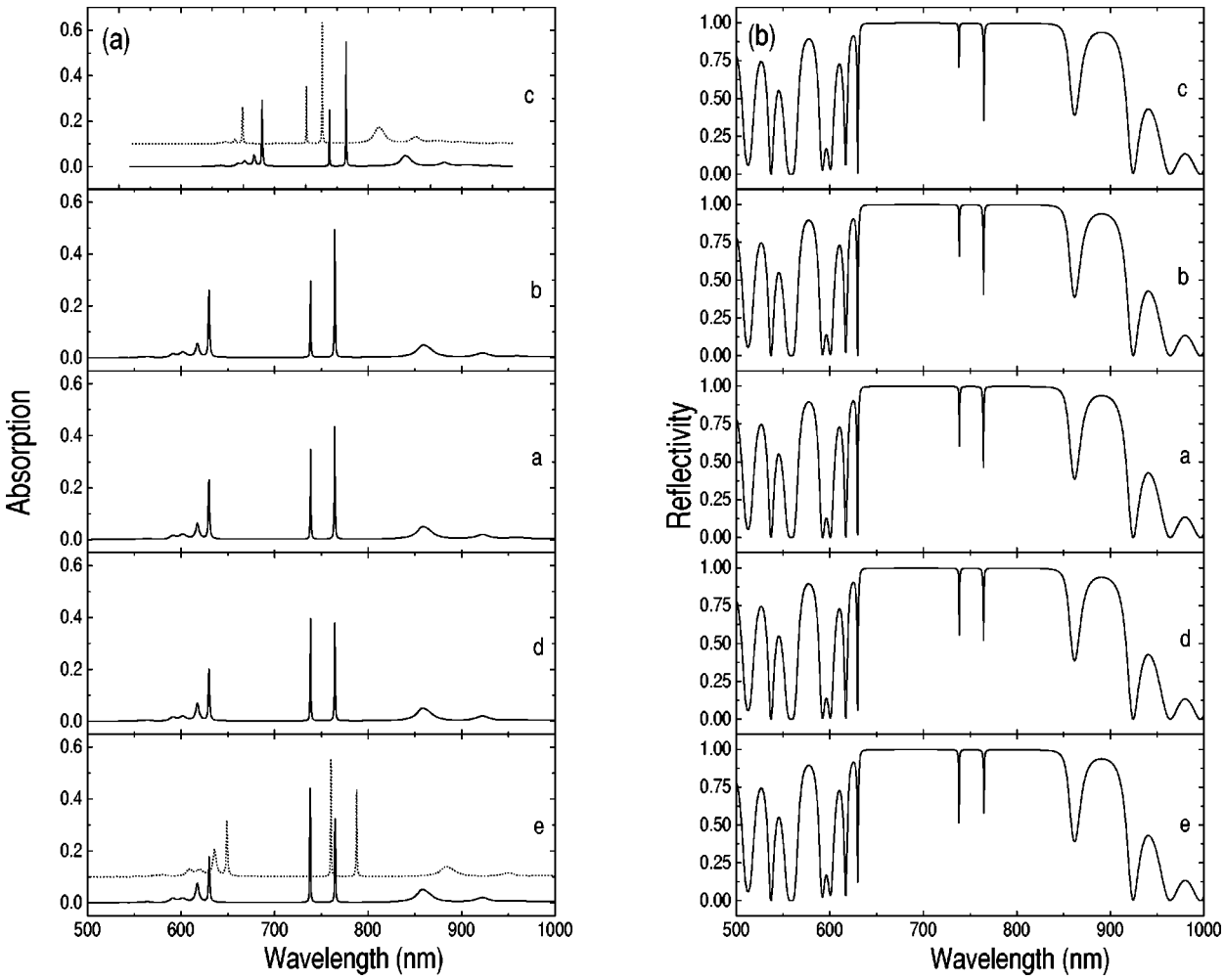

FIG. 6. (a) Absorption and (b) reflectivity spectra of the coupled microcavities for the same structures used in Fig. 3. Dotted curve in upper (lower) panel in (a): refractive indices reduced (increased) by 5% (3%). The labels on the spectra refer to the name of the various samples. Parameters of the calculation: see Table I and text.

the resonance frequency distribution when a finite value of γ is assumed; the precise value of γ is unimportant. Since the outer cavity S_1 gives the largest contribution to reflectivity and absorption spectra, when the outer cavity is thicker the peak at higher wavelength is more intense (samples *b* and *c*); on the other hand, when the outer cavity S_1 is thinner (samples *d* and *e*) the peak at lower wavelength becomes more pronounced. For a real refractive index this cannot be the case, since then time-reversal symmetry holds and the reflectivity of any structure (symmetric or not) is the same from both sides. Comparing with the experimental results shown in Fig. 3 we see that the qualitative features and the trends with increasing cavity mismatch are very well reproduced.

Obviously this calculation yields only minor changes of the peak positions with cavity mismatch. However, the peak positions are again very sensitive to the precise values of the refractive indices: a variation of a few percent changes the peak positions by several tens of nm. Comparison of different sets of samples shows that variation of peak positions by 30 nm are quite common and are simply due to the limitations in the control of the growth: thus the variations observed in Fig. 2 are just due to slight random deviations of the refractive indices from the nominal ones. In order to simulate this effect, the dotted lines in the upper (lower) panel of Fig. 6(a) show the reflectivity calculated by reducing (increasing) the refractive indices by 5% (3%), respectively: this calculation reproduces in a satisfactory way the experimental peak positions observed in Fig. 3.

V. CONCLUSIONS

The control of the etching process in PS allows the formation of coupled PSM's in which an energy splitting of the cavity resonances is observed, as in III-V coupled microcavities;[11,14] this shows that coherence of the optical modes is maintained over the whole structure, indicating the good optical quality of the material. Reflectivity spectra allow for a precise characterization of the coupled cavity peaks and of the stop band. Photoluminescence experiments for samples with varying mismatch between the two cavities show coupled cavity peaks with an asymmetry in intensity, which depends on both cavity mismatch and the presence of absorption. These findings agree well with the results of a theoretical model, in which the optical properties of the multilayer structure are simulated by assuming a distribution of frequencies for the quantized oscillators in the PS layers. While the precise peak line shape in both reflectivity and

photoluminescence depends on a number of material parameters and is almost independent of the properties of the emitters in the PS layers, the relative intensities of the various PL peaks allow to deduce the important parameter β, which is related to the oscillator strength and to the radiative recombination rate. The oscillator strength per cell is found to be $f_{\mathrm{cell}} \simeq 4 \times 10^{-5}$., i.e., quite small: this value is much lower than that of a direct gap material because the radiative transition in PS is induced by quantum confinement in indirect gap silicon nanocrystals. To our knowledge, this is the first determination of β not from time-resolved luminescence decay, where a crucial role is played by nonradiative recombination; the value of β provides further support for the model of luminescence from quantum confined states in Si quantum dots. The application of coupled PSM's for enhanced nonlinear optical effects is underway.

ACKNOWLEDGMENTS

L. P. wishes to acknowledge the skillful help of M. Cazzanelli, P. Dubos, and C. Vinegoni during the measurements. The authors are also grateful to A. V. Kavokin and V. Pellegrini for useful discussions. The experiments have been supported by CNR (Grant No. 97.01383.PF48). The fine Si wafers have been provided by MEMC Electronic Materials (Novara, Italy).

[1] L. T. Canham, Appl. Phys. Lett. **57**, 1046 (1990).
[2] A. G. Cullis, L. T. Canham, and P. D. J. Calcott, J. Appl. Phys. **82**, 909 (1997).
[3] C. Delerue, M. Lannoo, and G. Allan, J. Lumin. **57**, 249 (1993).
[4] B. Delley and E. F. Steigmeier, Phys. Rev. B **47**, 1397 (1993).
[5] See, e.g., *Confined Electrons and Photons: New Physics and Devices*, edited by E. Burstein and C. Weisbuch (Plenum, New York, 1995).
[6] H. Yokoyama, Y. Nambu, and T. Kawakami, in *Confined Electrons and Photons: New Physics and Devices* (Ref. 5), p. 427.
[7] G. Björk, Y. Yamamoto, and H. Heitmann, in *Confined Electrons and Photons: New Physics and Devices* (Ref. 5), p. 467; G. Björk and Y. Yamamoto, in *Spontaneous Emission and Laser Oscillation in Microcavities*, edited by H. Yokoyama and K. Ujihara (CRC Press, London, 1995), p. 189.
[8] V. Pellegrini, A. Tredicucci, C. Massoleni, and L. Pavesi, Phys. Rev. B **52**, 14 328 (1995).
[9] M. Cazzanelli and L. Pavesi, Phys. Rev. B **56**, 15 264 (1997).
[10] L. Pavesi, Nuovo Cimento **20**, 1 (1997).
[11] R. P. Stanley, R. Houdré, U. Oesterle, M. Ilegems, and C. Weisbuch, Appl. Phys. Lett. **65**, 2093 (1994).
[12] P. Michler, M. Hilpert, and G. Reiner, Appl. Phys. Lett. **70**, 2073 (1997).
[13] P. Pellandini, R. P. Stanley, R. Houdré, U. Oesterle, M. Ilegems, and C. Weisbuch, Appl. Phys. Lett. **71**, 864 (1997).
[14] A. Armitage *et al.* (unpublished).
[15] If $\lambda_1 = 620$ nm and $\lambda_2 = 840$ nm are taken as the limits of the stop band, we have $\lambda_s = 2\lambda_1\lambda_2/(\lambda_1 + \lambda_2)$, since the reflectivity spectrum is symmetric only when plotted against frequency.
[16] M. Born and E. Wolf, *Principles of Optics* (Pergamon, Oxford, 1960).
[17] H. A. McLeod, *Thin-Film Optical Filters*, 2nd ed. (Hilger, London, 1986).
[18] V. Savona, L. C. Andreani, A. Quattropani, and P. Schwendimann, Solid State Commun. **93**, 733 (1995).